Materials Advances

ROYAL SOCIETY OF CHEMISTRY

PAPER

View Article Online
View Journal | View Issue

Cite this: *Mater. Adv.*, 2026, 7, 2766

Tunable drug delivery *via* functionalized C_{18} nanorings: a DFT-MD investigation of 5-fluorouracil adsorption and release

Alaa M. Khudhair[ab] and Ali Ben Ahmed *[bc]

Nanomaterials have transformed the field of targeted drug delivery by providing exceptional surface-to-volume ratios, tunable electronic characteristics, and the potential for controlled release mechanisms. They can enhance treatment efficiency, reduce adverse effects, and increase bioavailability by precisely interacting with therapeutic molecules. This investigation investigates the electronic properties and adsorption behavior of 5-fluorouracil (FU) on pristine and doped C_{18} nanorings (B–C_{18}, N–C_{18}, and Si–C_{18}) using density functional theory (DFT) considering these advantages. Stable and thermodynamically advantageous physisorption is confirmed by the calculated adsorption energies (E_{ads}) of FU@B–C_{18} and FU@N–C_{18}, which range from −0.772 eV to −0.930 eV. The band structure is effectively customized by doping, as evidenced by the narrowest band gap (0.463 eV) in FU@Si–C_{18} compared to 1.861 eV in FU@C_{18}. This suggests that the electronic sensitivity has been enhanced. The Mulliken charge transfer (CT) analysis suggests that FU functions as an electron donor, with the highest charge transfer observed for FU@B–C_{18} (−0.060*e*). FU@B–C_{18} exhibits rapid desorption (9.3 s), while FU@N–C_{18} exhibits robust retention (4.2×10^3 s), indicating a balance between release efficiency and stability. Recovery time (τ) varies accordingly. The thermodynamic stability and structural integrity of the FU–C_{18} complexes are further confirmed by complementary molecular dynamics (MD) simulations, which guarantee dependable performance under physiological conditions. The potential of doped and functionalized C_{18} nanorings as advanced nanocarriers for FU cancer therapy is underscored by these findings.

Received 10th December 2025,
Accepted 26th January 2026

DOI: 10.1039/d5ma01445j

rsc.li/materials-advances

1. Introduction

Cancer is a significant global health concern in the 21st century, being the second highest cause of mortality globally. Recent estimates from the World Health Organization indicate that cancer was responsible for almost 10 million deaths in 2020, with forecasts suggesting a persistent increase in incidence due to aging populations, environmental exposures, and changing lifestyle factors.[1] The many characteristics of cancer, its ability to evade the immune system, and the development of treatment resistance all impede sustained therapeutic efficacy. Traditional chemotherapeutic techniques, while fundamental to clinical practice, often exhibit limited therapeutic windows and systemic toxicity, highlighting the need for more targeted and effective delivery methods.[2]

Nanotechnology has emerged as a breakthrough platform in oncology, allowing the strategic design of nanocarriers capable of encapsulating or adsorbing anticancer drugs, traversing biological barriers, and delivering their payload in a regulated and site-specific manner.[3] Ring-shaped or cyclic nanostructures, including cyclodextrins and other macrocyclic compounds, are crucial for drug delivery because they can form inclusion complexes with drug molecules. Improved solubility, stability, and bioavailability are achieved by encapsulating medications that are inadequately water-soluble in their distinctive cavities. These structures can also facilitate controlled release and safeguard pharmaceuticals from enzymatic degradation. Macrocyclic carriers that are functionalized can be customized to accomplish site-specific delivery, which can reduce adverse effects and improve therapeutic efficacy. These characteristics render them valuable platforms for advanced pharmaceutical applications, particularly in the fields of cancer therapy and targeted drug release systems.[4,5]

Carbon-based nanomaterials, including carbon nanotubes, graphene derivatives, fullerenes, and lately carbon nanorings, have garnered significant attention owing to their distinctive physicochemical features, elevated surface area-to-volume

[a] *Department of Physics, College of Science, University of Sumer, Iraq, Thi-Qar 64000, Iraq*
[b] *Department of Physics, College of Science, University of Sfax, Sfax 3000, Tunisia*
[c] *Department of Biomedical, Higher Institute of Biotechnology of Sfax, University of Sfax, Sfax 3000, Tunisia. E-mail: ali.benahmed@isbs.usf.tn*

ratios, and adjustable surface functions.[6] Carbon nanorings, which are distinguished by their cyclic π-conjugated architecture of sp^2-hybridized carbon atoms, provide a symmetrical substrate with a well-defined structure and strong π–π interaction potential for aromatic medicinal molecules, including 5-FU.[7] In comparison to planar graphene fragments, their curvature and topological characteristics also confer unique electronic properties.

Heteroatom doping and functionalization of C_{18} nanorings constitute an advanced atomic-scale engineering approach, facilitating precision modulation of structural, electronic, and interfacial characteristics. The introduction of dopants, including boron (B), nitrogen (N), and silicon (Si), enables the modification of the material's band gap, charge distribution, and adsorption sites, thereby directly affecting the adsorption strength of 5-fluorouracil (5-FU), charge transfer (CT) processes, and drug-release characteristics. This modification improves the capacity of C_{18} nanorings to enable targeted drug delivery, thereby optimizing the system's stability and responsiveness. Furthermore, these alterations in electronic characteristics facilitate the effective modulation of interactions with therapeutic agents, thereby enhancing the material's efficacy in the treatment of cancer. The influence of heteroatom doping on these characteristics has been extensively reported within the existing literature concerning dopant-based atomic-scale functionalization and electronic structure modification.[8–10]

5-Fluorouracil (5-FU) is a widely used chemotherapeutic agent for various solid tumors, yet its clinical efficacy is limited by poor selectivity, systemic toxicity, and rapid metabolic clearance. These limitations necessitate the development of nanocarriers capable of enhancing 5-FU's bioavailability and enabling controlled release.[11–13] Doping carbon-based nanomaterials with heteroatoms (*e.g.*, B, N, Si) is a well-established approach to modulate surface reactivity, improve adsorption behavior, and facilitate selective interactions with drug molecules.

Several theoretical and experimental investigations have already analyzed the impact of heteroatom substitutions on drug delivery efficacy.[14] Density functional theory (DFT) simulations have shown increased adsorption energies for anticancer medicines on nitrogen- or boron-doped graphene and carbon nanotube systems.[15] Likewise, silicon-doped carbon frameworks have shown potential in modulating electrostatic interactions and enhancing drug retention in adverse biological conditions.[16] Thus far, cyclic carbon nanorings have received little attention as a delivery platform, particularly regarding heteroatom doping and their relative efficacy as a 5-FU carrier.

Prior DFT-based investigations of drug carriers have mostly concentrated on expansive 2D sheets and inorganic nanocages (*e.g.*, graphene oxide, $Ca_{12}O_{12}$) or heteroatomic rings/cages (*e.g.*, C_3N_3/B_3O_3 and Al_8N_8/B_8N_8). This work investigates cyclocarbon (C_{18}) nanorings, a relatively unexplored cyclic carbon structure, and quantifies the modulation of interaction with 5-fluorouracil (FU) by heteroatom doping (B, N, and Si). We provide a comprehensive DFT–MD study that correlates adsorption energetics and charge transfer with electrical response, including band structure/DOS trends and work-function (Φ) modulation. Additionally, we evaluate the thermal stability of FU@C_{18} complexes by NVT molecular dynamics at 310 K. This framework delineates structure–property principles for doping-modulated FU binding and electrical behavior in cyclic carbon nanorings.

In this study, density functional theory (DFT) calculations are employed to investigate the adsorption properties, electronic characteristics, and reactivity profiles of 5-FU on pristine C_{18} and its doped derivatives (B–C_{18}, N–C_{18}, Si–C_{18}). Adsorption energies, band structures, density of states (DOS), global reactivity indices, Mulliken charge transfer, and molecular dynamics analyses were systematically performed to assess the influence of doping on FU binding affinity and carrier potential.

2. Computational methodology

We used *ab initio* calculations for computational design, structural improvement, and to check the main features of the structures we were looking at. These simulations used basis sets from a numerical linear combination of atomic orbitals (LCAO), supported by Quantum ATK software.[17–20]

To accurately model how adsorbed molecules and the substrate interact, we used the Perdew–Burke–Ernzerhof (PBE) generalized gradient approximation (GGA), along with van der Waals corrections (Grimme DFT-D3 parameters) for iterative calculations.[21–23] Computational methodology and *ab initio* molecular dynamics protocol. All density functional theory (DFT) calculations were conducted utilizing QuantumATK within the linear combination of atomic orbitals (LCAO) formalism. The simulation cell incorporated a vacuum region of 20 Å to mitigate artefactual interactions between periodic replicas. Brillouin zone sampling was performed at the Γ-point (1 × 1 × 1), and the real-space mesh cutoff was established at 150 Hartree. Convergence of the geometry optimizations was established when the total energy variation was less than 1×10^{-5} eV and the maximal residual force acting on any particle was below 0.01 eV $Å^{-1}$. Furthermore, *ab initio* molecular dynamics (AIMD) simulations were conducted to evaluate the finite-temperature stability of the FU–C_{18} complexes within the NVT ensemble at 310 K, employing a Nosé–Hoover thermostat (coupling time of 100 fs), a time step of 1.0 fs, and a total trajectory duration of 10 ps (following a 1 ps equilibration period). The 10 ps AIMD simulation window predominantly assesses the short-term thermal stability and endurance of FU-C_{18} contacts; however, uncommon desorption events and long-term release kinetics, which occur on nanosecond to microsecond timescales, are not comprehensively characterized within this timeframe. Consequently, *ab initio* molecular dynamics (AIMD) simulations serve as a qualitative assessment of stability, thereby augmenting the static density functional theory (DFT) analysis of adsorption energetics and electronic response. We also added PseudoDojo potentials[24] using the GGA for exchange and correlation.[25] The calculations were done using molecular dynamics simulation methods.

The following formulas are used to determine the Fermi level energy (E_{FL}) and electronic band gap (E_{gap}):[26–28]

$$E_g = E_{LUMO} - E_{HOMO} \quad (1)$$

E_{HOMO} signifies the energy level of the highest occupied molecular orbital, whereas E_{LUMO} represents the energy level of the lowest unoccupied molecular orbital.

The adsorption energy (E_{ads}) was determined by the following equation:[29,30]

$$E_{ads} = E_{FU-substrate} - E_{substrate} - E_{FU} \quad (2)$$

The global chemical reactivity descriptors are deduced using the following equations[31]:

$$IP = -E_{HOMO} \quad (3)$$

$$EA = -E_{LUMO} \quad (4)$$

$$H = \frac{E_{LUMO} - E_{HOMO}}{2} \quad (5)$$

$$S = \frac{1}{2\eta} \quad (6)$$

$$\mu = \frac{E_{LUMO} + E_{HOMO}}{2} \quad (7)$$

$$\omega = \frac{\mu^2}{2\eta} \quad (8)$$

The work function (Φ) represents a fundamental parameter in solid-state physics and surface science, extensively employed to characterize the energy barrier associated with electron emission from a material into the vacuum, as well as the electronic modifications induced by adsorption at surfaces.[32,33] In the current FU–C_{18} systems, Φ is utilized as an electronic-response descriptor that reflects the influence of heteroatom doping and 5-fluorouracil (FU) adsorption on the surface dipole and charge distribution of the nanoring, serving as a practical indicator for adjustable sensing signals and adsorption-induced carrier dynamics.

Consequently, Φ was determined from the electrostatic potential within the vacuum region and the Fermi level, as delineated in eqn (9).[34] To quantify the modulation induced by adsorption, the percentage variation in the work function was determined using eqn (10), wherein Φ_b and Φ_a represent the work function of the substrate prior to and following FU adsorption, respectively:

$$\Phi = V_{el(+\infty)} - E_{FL} \quad (9)$$

The symbol $V_{el(+\infty)}$ refers to the electrostatic potential of an electron at a significant distance from the surface, assumed to be zero (*i.e.*, $V_{el(+\infty)} = 0$).

We quantified the effect of FU adsorption on the work function utilizing eqn (10).

$$\Delta\Phi\ (\%) = \frac{\Phi_b - \Phi_a}{\Phi_b} \times 100 \quad (10)$$

The work function before and after adsorption is denoted by Φ_b and Φ_a, respectively.

The discussion surrounding recovery time (τ) underscores its significance in both drug delivery systems. By illuminating the relationship between recovery time and adsorption energy through traditional transition state theory, this study lays the groundwork for future technological advancements. Understanding these dynamics can lead to the creation of more responsive and efficient drug delivery methodologies. The insights gained from this exploration can drive innovations that significantly impact medical solutions:[35,36]

$$\tau = \frac{1}{\upsilon_0} e^{\frac{-E_{ads}}{k_B T}} \quad (11)$$

The variables in the equation are υ_0, which represents the attempt frequency, $k_B = 8.62 \times 10^{-5}$ eV K^{-1}, which is Boltzmann's constant, and T, which represents the temperature. The τ values at room temperature ($T = 298.15$ K) are determined using UV light ($\upsilon_0 = 10^{12}$ s^{-1}).

3. Results and discussion

3.1 Optimized geometries and structural features

The QuantumATK package was employed to conduct density functional theory (DFT) simulations to investigate the interactions between the FU anticancer drug and both pristine C_{18} and B-, N-, and Si-doped C_{18} substrates. The optimized geometries of the pristine and doped C_{18} structures are illustrated in Fig. 1 and 2, respectively, in both the absence and presence of the FU anticancer drug.

The overall ring structure of C_{18} maintains stability upon doping with B, N, or Si atoms, but some local distortions occur at the dopant site. The impact is more significant in the Si-doped structure owing to the greater atomic radius of silicon relative to carbon, as shown in Fig. 1.

The substrate comprises 18 carbon atoms (C_{18}) and is doped with diverse elements, such as boron, nitrogen, and silicon (B, N, Si). The optimized configurations, as illustrated in Fig. 2, indicate that the FU drug interacts with the pristine C_{18} substrate at distances of 2.89 Å (between the oxygen atom of the drug and a carbon atom of the substrate) and 2.80 Å (between the hydrogen atom of the drug and a carbon atom of the substrate). The O–B and H–C distances for the B-doped C_{18} system are 2.93 Å and 3.03 Å, respectively. In contrast, the O–N and H–C distances for the N-doped substrate are both 2.97 Å. In contrast, the Si-doped substrate exhibits interaction distances of 2.82 Å (H–C) and 3.13 Å (O–Si).

In addition, for the lowest energy structures, vibrational calculations were performed inside the harmonic approximation to confirm the identification of local minima and as a measure of structural stability; the results showed positive values, as shown in Fig. 3 and 4.

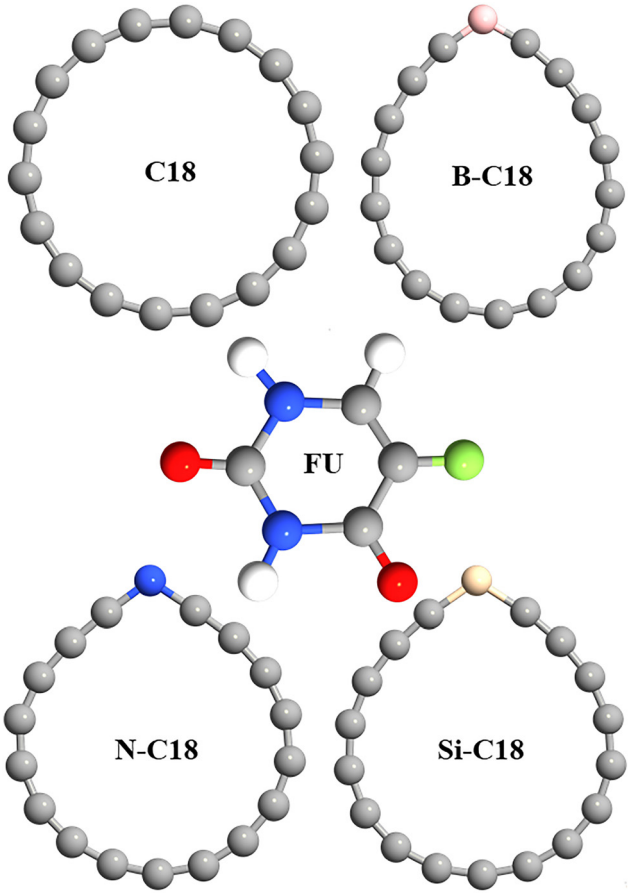

Fig. 1 Optimized geometries of the FU drug and C_{18} ring and doped derivatives.

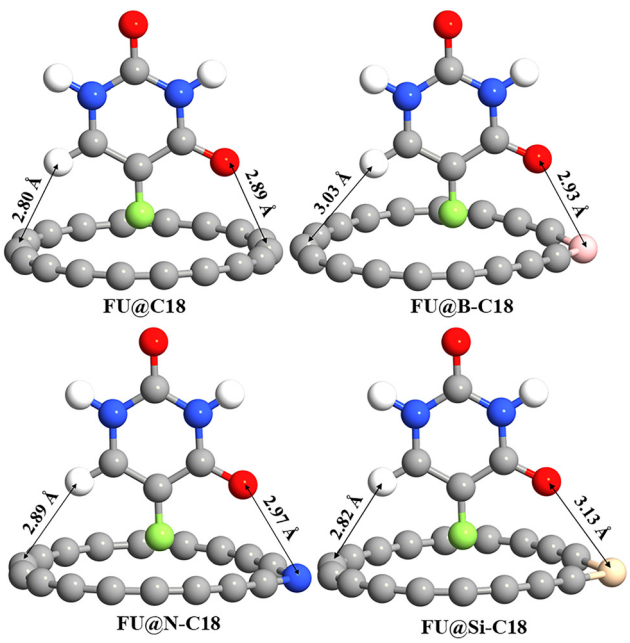

Fig. 2 Optimized geometries of the FU drug with C_{18} ring and doped derivatives.

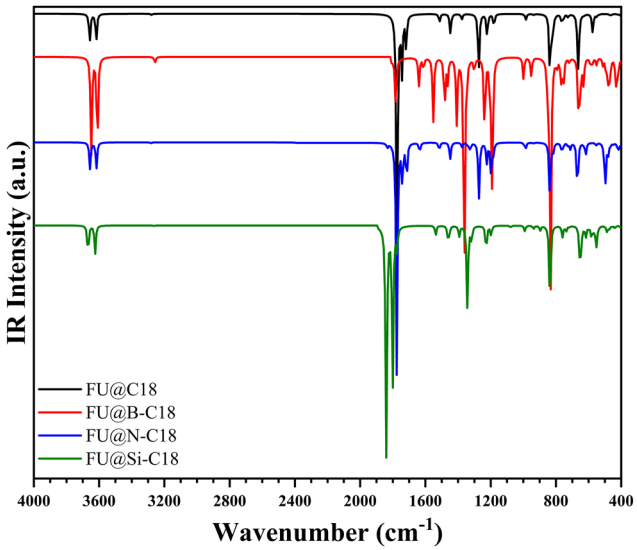

Fig. 3 IR spectra of FU@C_{18}, FU@B–C_{18}, FU@N–C_{18}, and FU@Si–C_{18}.

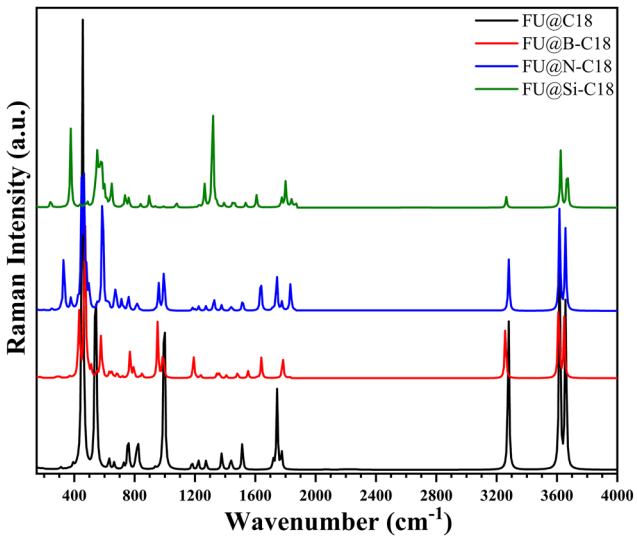

Fig. 4 IR spectra of FU@C_{18}, FU@B–C_{18}, FU@N–C_{18}, and FU@Si–C_{18}.

3.2 The electronic properties

The band structure diagrams in Fig. 5 and 6(a)–(d) demonstrate significant changes in the electronic characteristics of the various functionalized and doped C_{18}-based structures.

The total energy (E) values in Table 1 provide essential insights into the thermodynamic stability of the virgin, doped, and FU-functionalized C_{18} structures. Pristine C_{18} demonstrates the lowest total energy among the analyzed systems, indicating its fundamentally stable form. Doping with B, N, or Si results in a little elevation in total energy, attributable to lattice deformation and the incorporation of impurity atoms that alter the local electronic environment. Among the doped systems, Si–C_{18} exhibits the most significant rise in E, indicative of Si's larger atomic radius relative to C and the enhanced structural relaxation necessary for stability. For FU-functionalized

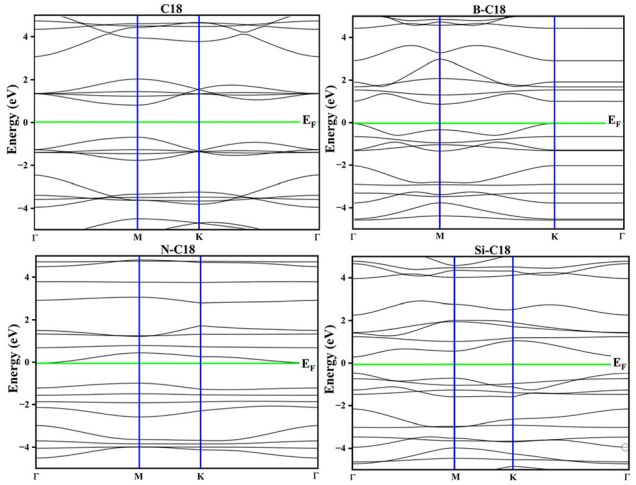

Fig. 5 Band structures of the C_{18} ring and doped derivatives.

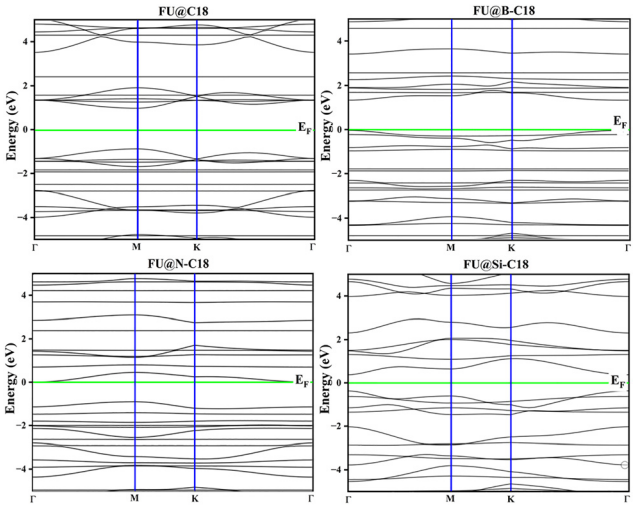

Fig. 6 Band structures of the Fu drug with C_{18} ring and doped derivatives.

C_{18} ($FU@C_{18}$), the total energy is marginally less negative than that of pristine C_{18}, indicating that the adsorption of FU groups induces more structural strain and electron redistribution. The combination of FU functionalization with doping ($FU@B–C_{18}$, $FU@N–C_{18}$, $FU@Si–C_{18}$) results in an increased total energy, indicating that the synergistic effects of functionalization and doping need more structural modifications to attain equilibrium. Nonetheless, the total energy remains negative across all configurations, affirming their thermodynamic viability and promise for experimental realization. These patterns suggest that whereas doping and FU functionalization somewhat diminish the thermodynamic stability compared to pure C_{18}, they provide considerable electrical tunability, as shown by the band structure, HOMO–LUMO levels, and DOS profiles.

The band structure of pure C_{18} has a significant energy gap of 1.47 eV, as shown in Table 1, signifying semiconducting characteristics with distinctly differentiated valence and conduction bands. Doping with B, N, or Si ($B–C_{18}$, $N–C_{18}$, and $Si–C_{18}$) results in a significant reduction in the energy gap, with the minimum gap of 0.736 eV recorded for $Si–C_{18}$. These substantial decreases, especially with Si doping (ΔE_g = −92.66%), indicate that these dopants create states proximate to the Fermi level, hence promoting electronic transitions and improving conductivity.

Functionalization with FU groups ($FU@C_{18}$), seen in Fig. 5a, results in an expansion of the energy gap (1.861 eV), suggesting that FU functionalization enhances the semiconducting properties of the structure. When FU groups are amalgamated with dopants (refer to Fig. 5b–d for $FU@B–C_{18}$, $FU@N–C_{18}$, and $FU@Si–C_{18}$), the band gaps are significantly reduced (1.361 eV, 0.896 eV, and 0.463 eV, respectively), hence affirming the substantial impact of dopant-induced states that prevail over the influence of FU. The HOMO and LUMO level placements shown in Table 1 align with these patterns.

The HOMO and LUMO levels of $N–C_{18}$ are nearer to the Fermi level than those of pure C_{18}, indicating a decreased gap of 0.914 eV. In contrast, $FU@C_{18}$ exhibits a more significant distinction between the HOMO and LUMO levels, aligning with its greater energy gap. These findings demonstrate that regulated doping (B, N, Si) and FU functionalization may effectively modify the electrical characteristics of the C_{18} structures. Doping lowers the band gap and improves conductivity, while FU functionalization may either restore or augment semiconducting properties, making these materials viable candidates for electrical and optoelectronic applications.

The density of states (DOS) profiles shown in Fig. 7 provide enhanced understanding of the electrical structure, supplementing the band structure diagrams presented in Fig. 5 and 6(a)–(d). The density of states (DOS) for pure C_{18} reveals a significant separation between the valence and conduction bands, exhibiting few states at the Fermi level, hence affirming its semiconducting characteristics and a band gap of 1.47 eV (Table 1). This characteristic aligns with other carbon-based nanostructures, whereby a substantial HOMO–LUMO gap enhances electrical stability and diminishes intrinsic conductivity.

Doping with heteroatoms like B, N, or Si significantly modifies the density of states, creating localized states near the Fermi energy. This leads to a significant decrease in the band gap, particularly for $Si–C_{18}$ (0.736 eV), where distinct peaks at E_F signify improved conductivity owing to the heightened density of available states. Comparable phenomena have been found in doped graphene systems.

In FU-functionalized C_{18} ($FU@C_{18}$), the band gap rises to 1.861 eV, accompanied by a reduction in states at the Fermi level, hence enhancing its semiconducting characteristics. The synergistic impact of FU groups and doping ($FU@B–C_{18}$), $FU@N–C_{18}$ $FU@Si–C_{18}$ reintroduces states next to the Fermi level, reducing the energy gap and altering the distribution of the density of states. This illustrates how doping and functionalization may collaboratively regulate the band structure and density of states (DOS).

3.3 Adsorption energy and charge transfer

The adsorption energy (E_{ads}) and charge transfer (CT) are essential metrics for comprehending the interaction between

Table 1 The values of the total energy (E), Fermi level energy (E_{FL}), work function (Φ), E_{HOMO}, E_{LUMO}, and energy gap (E_g) for the structures in (eV) units

Structure	E	E_{FL}	Φ	$\Delta\Phi$ (%)	E_{HOMO}	E_{LUMO}	E_g	ΔE_g (%)
C_{18}	−2799.183	−7.766	7.766	—	−8.460	−6.991	1.470	—
B–C_{18}	−2719.441	−7.713	7.713	−0.68	−7.714	−6.827	0.887	−39.66
N–C_{18}	−2915.523	−7.838	7.838	0.92	−8.753	−7.839	0.914	−37.82
Si–C_{18}	−2815.761	−7.539	7.539	−2.92	−7.910	−7.174	0.736	−92.66
FU@C_{18}	−5533.383	−7.724	7.724	−0.54	−8.598	−6.737	1.861	26.60
FU@B–C_{18}	−5453.679	−7.853	7.853	1.12	−7.880	−6.519	1.361	−7.41
FU@N–C_{18}	−5649.895	−7.699	7.699	−0.86	−8.596	−7.700	0.896	−39.04
FU@Si–C_{18}	−5550.038	−7.621	7.621	−1.86	−7.872	−7.409	0.463	−68.50

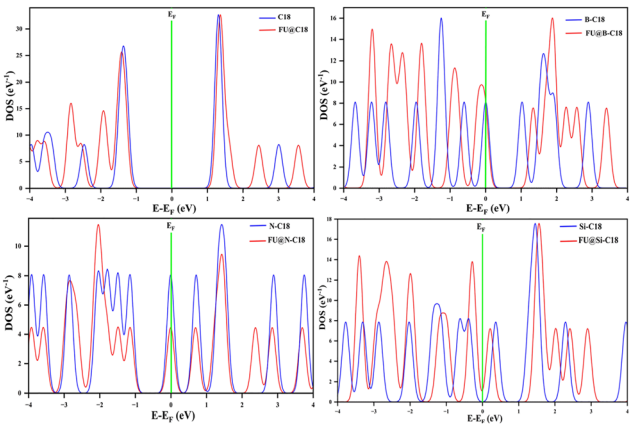

Fig. 7 Density of states (DOS) of pristine and doped graphene surfaces before and after FU adsorption.

a molecule and a substrate, as they directly influence the stability, electronic characteristics, and possible sensing efficacy of the system. E_{ads} assesses the thermodynamic favorability and binding strength of adsorption, whereas CT measures the degree of electronic exchange, offering critical insights into reactivity and surface activity.

The adsorption energies shown in Table 2 are uniformly negative, indicating that FU adsorption on both pure and doped C_{18} surfaces is exothermic and thermodynamically advantageous. FU@N–C_{18} demonstrates the most robust interaction (−0.930 eV), ascribed to the significant electronic coupling resulting from nitrogen doping. Conversely, FU@B–C_{18} has the least negative E_{ads} (−0.772 eV), signifying weaker binding, whilst FU@C_{18} and FU@Si–C_{18} have intermediate values (−0.824 eV and −0.812 eV), illustrating that doping efficiently modulates adsorption strength.

The Mulliken study reveals that charge transfer occurs from FU to the C_{18}-based surfaces, as shown by the negative CT values. A negative CT indicates that the FU molecule functions as an electron donor, while the C_{18} surface operates as an electron acceptor, aligning with observations documented for analogous functionalized carbon systems.[37] The maximum charge transfer (CT) is recorded for FU@B–C_{18} (−0.060e), followed by FU@Si–C_{18} (−0.053e), whilst FU@C_{18} and FU@N–C_{18} demonstrate lower charge transfers of −0.011e and −0.036e, respectively. This pattern indicates that dopants such as B and Si augment the charge exchange process, thus affecting the electrical reactivity of the surface. These results align with publications on doped carbon nanostructures, whereby charge transfer (CT) is crucial for improving sensing and catalytic efficacy. The sign of the charge transfer (CT) values indicates the donor–acceptor characteristics of the system. A negative CT value indicates that electrons are transported from the adsorbed molecule (FU) to the C_{18}-based substrate, indicating that FU functions as the electron donor, whilst the C_{18} surface serves as the electron acceptor. If the CT value were positive, the substrate would function as the donor and the molecule as the acceptor. The current work indicates that all CT values are negative (Table 2), thus demonstrating that electron transport transpires from FU to both pure and doped C_{18} surfaces, aligning with donor–acceptor interactions documented in analogous carbon nanostructures.[38,39]

Table 2 The adsorption energy (E_{ads}), Mulliken CT, and the recovery time for all complex structures

Structures	E_{ads} (eV)	BSSE correction	CT	τ (s)	σ (A m^{-2})
FU@C_{18}	−0.824	0.525	−0.011	7×10^{1}	1.170×10^{-6}
FU@B–C_{18}	−0.772	0.630	−0.060	9.3×10^{0}	1.964×10^{-2}
FU@N–C_{18}	−0.930	0.578	−0.036	4.2×10^{3}	1.66×10^{2}
FU@Si–C_{18}	−0.812	0.604	−0.053	4.4×10^{1}	7.60×10^{5}

Electrical conductivity (σ) is a fundamental feature associated with adsorption behavior, charge transfer (CT), and band gap, indicating a material's capacity to conduct electricity. Table 2 illustrates that the conductivity (σ) of FU@C_{18} systems exhibits considerable variation, with FU@C_{18} measuring 1.170×10^{-6} A m^{-2}, while FU@Si–C_{18} attains 7.60×10^{5} A m^{-2}. The reduced conductivity of FU@C_{18} aligns with its comparatively broad band gap (1.861 eV), limiting charge carrier movement. Conversely, the elevated conductivity of FU@Si–C_{18} is ascribed to the pronounced electron delocalization resulting from Si doping and a markedly decreased band gap of 0.463 eV. FU@N–C_{18} exhibits significant conductivity (1.66×10^{2} A m^{-2}), consistent with its intermediate band gap (0.896 eV) and elevated electron density. Boron doping in FU@B–C_{18} ($\sigma = 1.964 \times 10^{-2}$ A m^{-2}) improves conductivity relative to FU@C_{18}, however its impact is less significant than that of silicon or nitrogen doping. The observations demonstrate a distinct correlation among σ, CT, and band gap: reduced band gaps and enhanced electron transport (more negative CT) result in increased conductivity. The work function ($\Delta\Phi$) indirectly influences σ by affecting electron emission and carrier availability. The results indicate that Si and N doping significantly improve

conductivity, essential for nanoelectronics, sensors, and catalytic systems. The tunability underscores the promise of FU-functionalized C_{18} derivatives as multifunctional materials, tailored for adsorption stability and electrical responsiveness.

3.4 Work function (Φ) and its modification

Recent DFT/MD investigations into nanoscale drug-carrier systems have underscored that adsorption affinity, and charge-transfer characteristics serve as valuable design parameters for modulating nanocarrier performance, including in the case of 5-fluorouracil. Building upon these recent advancements, we analyze the current FU–C1T findings by correlating adsorption energetics with charge transfer (CT) and the related electronic perturbation, whereas the work-function response is addressed independently in the dedicated Φ section.[40–42]

The work function (Φ), which is the minimal energy required to extract an electron from the Fermi level to the vacuum, is a crucial parameter influencing the surface electrical behaviour, field emission characteristics, and sensing capacities of carbon-based nanomaterials.[43] In these systems, little variations in Φ may substantially modify the electrical response, becoming a crucial element in the development of chemical sensors, nanoelectronics, and catalytic devices.[44] Chemical perturbations, such as doping or molecule adsorption, cause charge redistribution and surface dipole production, leading to a shift in the Fermi level and observable alterations in Φ.[45]

The data presented in Table 1 indicate that pure C_{18} has a work function of 7.766 eV. Boron doping marginally decreases Φ to 7.713 eV ($\Delta\Phi$ = −0.68%), signifying modest electron donation, whereas nitrogen doping elevates it to 7.838 eV ($\Delta\Phi$ = +0.92%) owing to its electron-withdrawing properties.[46] Silicon doping results in the most significant reduction, producing a Φ of 7.539 eV ($\Delta\Phi$ = −2.92%), which correlates with a rise in surface electron density. The functionalization with FU groups further adjusts Φ, with FU@C_{18} demonstrating a marginally reduced value of 7.724 eV ($\Delta\Phi$ = −0.54%). The variance becomes more pronounced when dopants are included, with FU@B–C_{18} attaining 7.853 eV (+1.12%), but FU@N–C_{18} and FU@Si–C_{18} decrease to 7.699 eV (−0.86%) and 7.621 eV (−1.86%), respectively[47] (see Fig. 8).

An important discovery is that the sign and magnitude of $\Delta\Phi$ are correlated with the charge transfer (CT) values. Systems exhibiting negative CT (electron transport from FU to the surface) often show a decrease in Φ because of the heightened surface electron density. Conversely, when $\Delta\Phi$ is positive (*e.g.*, FU@B–C_{18}), the surface exhibits characteristics akin to an electron acceptor, indicating enhanced electron-withdrawing effects. A high $\Delta\Phi$ promotes sensor sensitivity by elevating the energy barrier for electron emission, whereas a low $\Delta\Phi$ boosts field emission and catalytic activity by augmenting electron availability.[48]

The electronic behavior of pristine and doped C_{18} systems is comprehensively understood through the interplay between adsorption energy (E_{ads}), charge transfer (CT), and work function variation ($\Delta\Phi$). Stronger molecule–surface interactions are typically associated with a more negative E_{ads}, which is frequently accompanied by higher CT values because of increased electronic coupling. Electron transfer from the FU molecule to the surface is indicated by negative CT values, and typically reduces Φ (negative $\Delta\Phi$) by increasing the density of surface electrons, as demonstrated in FU@Si–C_{18} and FU@N–C_{18}. In contrast, systems with positive $\Delta\Phi$, such as FU@B–C_{18}, demonstrate electron-withdrawing behavior, resulting in a slight increase in Φ and an enhanced sensing potential. The simultaneous tailoring of E_{ads}, CT, and Φ can be strategically employed to optimize both adsorption stability and electronic response for targeted applications in sensing, catalysis, and nanoelectronics, as these correlations highlight.

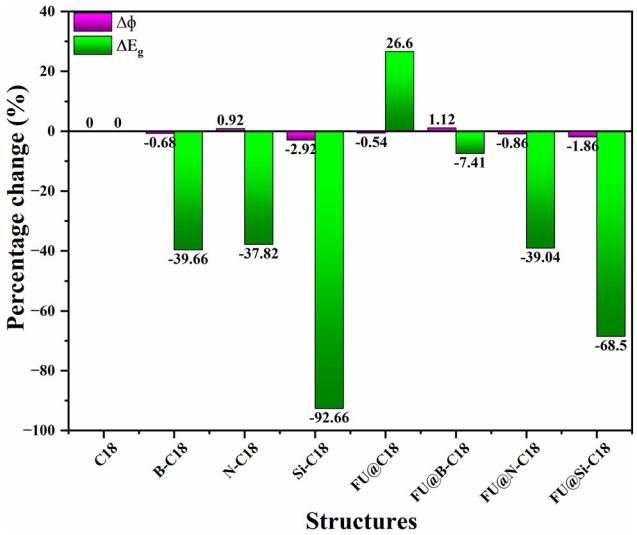

Fig. 8 Percentage variation in work function ($\Delta\Phi$) and energy gap (ΔE_g) for pristine, doped, and FU-functionalized C_{18} structures.

3.5 Recovery time

The recovery time (τ) is a critical measure in assessing material performance for applications like medication administration and gas sensing, since it denotes the duration needed for the adsorbed FU molecule to disengage from the surface and restore the substrate to its original condition. The values of τ are directly affected by the adsorption energy (E_{ads}) (see Fig. 9), with stronger adsorption generally leading to an extended recovery time owing to the enhanced stability of the adsorbate–substrate combination.

Table 2 indicates notable discrepancies in recovery time between the pristine and doped C_{18} structures. FU@N–C_{18} has the greatest recovery duration (4.2×10^3 s), correlating with the highest adsorption energy (−0.930 eV). The robust interaction indicates that the desorption of FU from N-doped C_{18} may need a prolonged duration, thus limiting its use in scenarios requiring rapid reaction and regeneration. Conversely, FU@B–C_{18} exhibits the briefest recovery time (9.3×10^0 s) owing to its comparatively lower binding energy (−0.772 eV), rendering it beneficial for dynamic applications that need rapid adsorption and desorption cycles.

The intermediate values of τ for FU@C_{18} (7×10^1 s) and FU@Si–C_{18} (4.4×10^1 s) indicate moderate binding energies

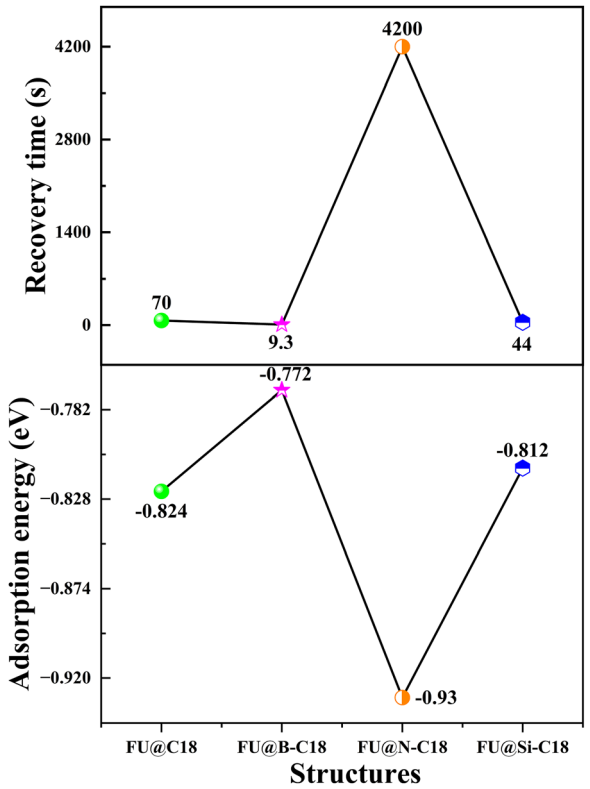

Fig. 9 Recovery time (τ) for FU adsorption on pristine and doped C_{18} structures.

(−0.824 eV and −0.812 eV, respectively), suggesting a balanced compromise between stability and reversibility. These patterns underscore the need of customizing adsorption strength to get optimum recovery durations. Although elevated adsorption energies improve the stability of the drug-surface interface, they may impede desorption, thereby diminishing system efficiency, particularly in sensing and drug delivery applications. This behavior aligns with previous research on functionalized and doped carbon nanostructures, which has highlighted the regulation of adsorption strength as a crucial element for enhancing recovery dynamics.[49]

3.6 Global reactivity indices

The global reactivity indices (shown in Table 3) provide essential insights into the electrical reactivity and stability of both pure and modified C_{18} structures. These factors are often used to forecast chemical behavior, donor–acceptor proclivities, and the suitability of materials for catalytic and sensing applications. They originate from frontier molecular orbital theory.[50,51]

Table 3 Global chemical reactivity descriptors

Structure	IP	EA	S	H	μ	ω
C_{18}	8.460	6.991	0.680	0.735	7.725	40.609
B–C_{18}	7.714	6.827	1.128	0.443	7.270	59.598
N–C_{18}	8.753	7.839	1.094	0.457	8.296	75.265
Si–C_{18}	7.910	7.174	1.358	0.368	7.542	77.262
FU@C_{18}	8.598	6.737	0.537	0.930	7.668	31.594
FU@B–C_{18}	7.880	6.519	0.735	0.680	7.200	38.093
FU@N–C_{18}	8.596	7.700	1.116	0.448	8.148	74.096
FU@Si–C_{18}	7.872	7.409	2.161	0.231	7.641	126.142

The ionization potential (IP) and electron affinity (EA), denoting the energy necessary to remove an electron and the energy acquired by adding an electron, respectively, reflect electronic stability. The immaculate C_{18} structure has an ionization potential of 8.460 eV and an electron affinity of 6.991 eV, indicating considerable electronic stability. Doping with boron or silicon decreases the ionization potential (7.714 eV for B–C_{18} and 7.910 eV for Si–C_{18}), signifying enhanced propensity for electron donation, advantageous for charge-transfer applications. Conversely, N–C_{18} has the greatest ionization potential (8.753 eV) and electron affinity (7.839 eV), indicating enhanced electron-accepting characteristics.

The oxidative stability of FU@C_{18} is enhanced by the slight elevation in ionization potential (8.598 eV) resulting from the functionalization with FU groups. The softness (S) and hardness (H) serve as inverse indicators of chemical reactivity, with higher S values signifying enhanced reactivity. Si–C_{18} demonstrates peak softness (1.358 eV^{-1}) and minimal hardness (0.368 eV), indicating increased chemical reactivity. FU@C_{18} has the lowest softness (0.537 eV^{-1}), indicating enhanced stability and less reactivity after FU functionalization. The electron-accepting characteristics of N–C_{18} (8.296 eV) and FU@N–C_{18} (8.148 eV) are shown by their elevated chemical potential (μ), indicating a propensity for electron ejection from the structure. In contrast, B–C_{18} and FU@B–C_{18} have reduced μ values (7.270 eV and 7.200 eV, respectively), corroborating their electron-donating characteristics.

The electrophilicity index (ω), which measures stability with the acquisition of an extra charge, differs across the systems. Si–C_{18} and FU@Si–C_{18} have the highest values (77.262 and 126.142, respectively), indicating robust electron uptake. The lowest ω (31.594) is recorded in FU@C_{18}, indicating a reduction in electrophilicity attributed to FU passivation.

In general, these global reactivity indices indicate that doping, especially with Si or N, increases the electrical reactivity and electron-accepting capacity of C_{18}, whereas FU functionalization stabilizes the structure and diminishes its electrophilicity. These characteristics render the systems exceptionally appropriate for electrical device engineering, catalysis, and sensing applications.[52]

3.7 Molecular dynamics

Molecular dynamics simulations were utilized to investigate the thermal stability of the FU@C_{18} complexes. Specifically, four independent NVT *ab initio* molecular dynamics (AIMD) trajectories were conducted at 310 K to assess whether the optimized adsorption configurations maintain their structural integrity under thermal fluctuations. The comprehensive AIMD protocol and all computational parameters, including the thermostat scheme, time step, and trajectory duration, are documented in Section 2 (Computational methodology) to consolidate the simulation details in a single section. The discussion below, therefore, concentrates on the observed trajectory behaviour and stability characteristics during the simulations.

The four different molecular dynamics simulations (Fig. 10 and 11) consistently show that the FU delivery system undergoes rapid thermal and energetic equilibration after initialization. Randomized initial velocity distributions are associated with the abrupt temperature increases that are observed at the commencement of each cycle. According to thermodynamic predictions for solvated molecular systems[53], the system stabilizes within sub-picosecond timescales, achieving equilibrium with the reservoir temperature within approximately 0.3–0.6 ps. A local energy minimum indicative of configurational relaxation is suggested by the stabilization of potential energy, which also occurs within similar timescales.

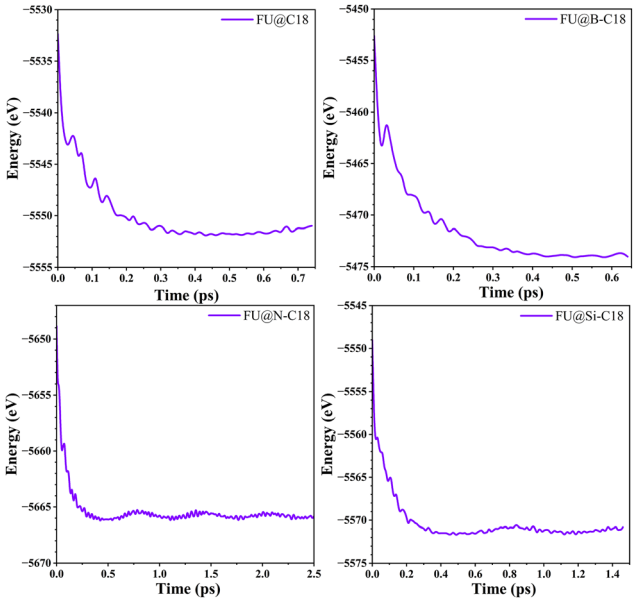

Fig. 10 Molecular dynamics trajectories depicting conformational transitions: potential energy stabilization.

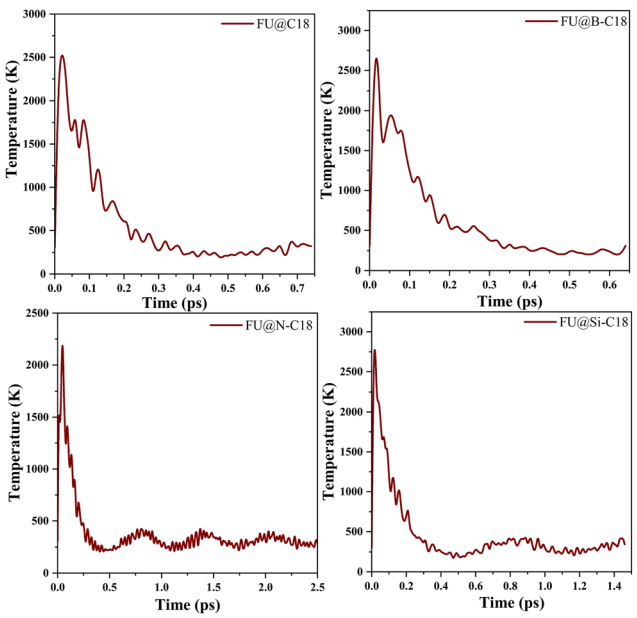

Fig. 11 Molecular dynamics trajectories depicting conformational transitions: temperature convergence.

The consistent equilibration behavior seen in all four tests reinforces the reliability of the FU delivery arrangement. The efficacy of the Nosé–Hoover thermostat in properly modeling canonical ensemble dynamics has been substantiated in prior investigations,[54] and a thermostat relaxation duration of 100 fs has shown effectiveness for thermal coupling without the introduction of artifacts. The observed thermal behavior corresponds with results from analogous research on drug encapsulation and release utilizing nanoscale carriers.[55] Therefore, our simulations demonstrate that the FU delivery system maintains stable dynamic behavior during physiologically relevant heat circumstances, and the used methodological framework may be dependably utilized for future investigation of transport, diffusion, and absorption processes.

We observe that the 10 ps AIMD trajectories are predominantly designed to serve as a brief assessment of the thermal stability of the FU@C_{18} complexes. Extended stability, infrequent desorption events, and release kinetics may manifest over prolonged (nanoseconds to microseconds) time scales and are consequently outside the scope of the current simulation window.

3.8 Biological feasibility and environmental stability considerations

The biocompatibility of C_{18} nanorings has been investigated in numerous studies, demonstrating minimal cytotoxicity in human cells, thereby suggesting their potential utility in biomedical applications. The incorporation of heteroatoms, including boron (B), nitrogen (N), and silicon (Si), improves biocompatibility. These modifications subtly alter the electronic characteristics of the nanorings, thereby optimizing their interactions within biological systems. Furthermore, multiple investigations have indicated that C_{18} nanorings demonstrate robust stability within aqueous environments, exhibiting negligible degradation across brief to intermediate durations, thereby rendering them appropriate for drug delivery and sensing applications.[56,57]

Nevertheless, the toxicity of C_{18} nanorings necessitates additional research, especially regarding prolonged exposure and potential bioaccumulation. Recent investigations indicate that surface functionalization employing specific moieties, including FU groups, may attenuate the toxicity of nanostructures by diminishing cellular harm and enhancing their selective absorption within target tissues.[58,59] The effect of these alterations on the comprehensive toxicity profile necessitates assessment within more sophisticated *in vitro* and *in vivo* models.

To evaluate the stability under physiological conditions, molecular dynamics (MD) simulations were conducted to examine the behavior of C_{18} within simulated biological fluids. The simulations indicate that C_{18} nanorings exhibit considerable stability within biological environments over a brief duration. However, additional long-term simulations, extending from nanoseconds to microseconds, are required to comprehensively

assess their behavior and degradation characteristics under authentic physiological conditions.[59–61]

4. Conclusion

In this study, DFT was employed to conduct a comprehensive theoretical analysis of the electronic properties and adsorption of 5-fluorouracil (FU) on pristine and doped C_{18} nanorings (B–C_{18}, N–C_{18}, and Si–C_{18}). The results indicate that the electronic structure and adsorption characteristics of C_{18} nanorings can be precisely tailored through the use of doping and FU functionalization. The adsorption energies (E_{ads}) that were calculated, which range from −0.772 eV for FU@B–C_{18} to −0.930 eV for FU@N–C_{18}, confirm the thermodynamic stability and moderate binding strength of the compounds. These properties are perfect for reversible drug loading and release.

The band gap has been significantly reduced, particularly for FU@Si–C_{18} (0.463 eV), which suggests that the electronic responsiveness has been improved. The recovery time (τ) analysis has revealed a complex equilibrium between rapid desorption (τ = 9.3 s for FU@B–C_{18}) and strong adsorption ($\tau = 4.2 \times 10^3$ s for FU@N–C_{18}). This allows for the tunable release of the drug. The Mulliken charge transfer (CT) analysis further demonstrates that FU functions as an electron donor, thereby modulating the surface reactivity of the nanorings. In addition, the structural stability of FU–C_{18} complexes under thermal fluctuations is further validated by complementary molecular dynamics (MD) simulations, which further supports their reliability for biomedical applications. The potential of doped C_{18} nanorings as versatile substrates for drug delivery and nanosensing is underscored by this work, which also offers fundamental insights into the adsorption mechanism of anticancer medications on carbon-based nanomaterials. The development of next-generation nanocarriers is facilitated by the combination of controllable electronic tuning and stable and reversible adsorption in these nanostructures. This approach allows for the optimization of efficiency, selectivity, and adaptability for advanced biomedical applications.

Author contributions

All authors contributed to the conception and design of the study. Alaa M. Khudhair performed material preparation, computations, data collection and analysis and Ali Ben Ahmed supervised this study. All authors discussed the results and contributed to reading and approving the final manuscript.

Conflicts of interest

There are no conflicts to declare.

Data availability

Supplementary information (SI) is available. The optimized structures FU@C18, FU@B-C18, FU@N-C18 and FU@Si-C18. See DOI: https://doi.org/10.1039/d5ma01445j.

References

1 H. Sung, *et al.*, Global cancer statistics 2020: GLOBOCAN estimates of incidence and mortality worldwide for 36 cancers in 185 countries, *CA-Cancer J. Clin.*, 2021, **71**(3), 209–249.
2 S. K. Chakrabarti and D. Chattopadhyay, Cancer Immunotherapy: Bridging Concept with Practice–A Broad-Brush Stroke, *Health*, 2024, **5**(3), 1108.
3 R. Singh and J. W. Lillard Jr, Nanoparticle-based targeted drug delivery, *Exp. Mol. Pathol.*, 2009, **86**(3), 215–223.
4 S. V. Kurkov and T. Loftsson, Cyclodextrins, *Int. J. Pharm.*, 2013, **453**(1), 167–180.
5 T. Loftsson and D. Duchene, Cyclodextrins and their pharmaceutical applications, *Int. J. Pharm.*, 2007, **329**(1–2), 1–11.
6 S. Iijima, Helical microtubules of graphite carbon, *Nature*, 1999, **56**, 354.
7 S. Yamago, E. Kayahara and T. Iwamoto, Organoplatinum-Mediated Synthesis of Cyclic π-Conjugated Molecules: Towards a New Era of Three-Dimensional Aromatic Compounds, *Chem. Rec.*, 2014, **14**(1), 84–100.
8 H. Kurban, S. Alaei and M. Kurban, Effect of Mg content on electronic structure, optical and structural properties of amorphous ZnO nanoparticles: A DFTB study, *J. Non-Cryst. Solids*, 2021, **560**, 120726–120732, DOI: 10.1016/j.jnoncrysol.2021.120726.
9 H. Kurban, P. Sharma, M. M. Dalkilic and M. Kurban, Accelerating density of states prediction in Zn-doped MgO nanoparticles via kernel-optimized weighted k-NN, *Sci. Rep.*, 2025, **15**(1), 30524, DOI: 10.1038/s41598-025-07887-6.
10 Z. Shariatinia and M. Kurban, Sustainable design of green-functionalized-conjugated BTBF-DPA derivatives for high-mobility hole transport, *Tetrahedron*, 2025, **188**, 134984–134994, DOI: 10.1016/j.tet.2025.134984.
11 G. J. Ogunwale, *et al.*, Interaction of 5-fluorouracil on the surfaces of pristine and functionalized $Ca_{12}O_{12}$ nanocages: an intuition from DFT, *ACS Omega*, 2023, **8**(15), 13551–13568.
12 F. Safdari, H. Raissi, M. Shahabi and M. Zaboli, DFT calculations and molecular dynamics simulation study on the adsorption of 5-fluorouracil anticancer drug on graphene oxide nanosheet as a drug delivery vehicle, *J. Inorg. Organomet. Polym. Mater.*, 2017, **27**(3), 805–817.
13 Z. Yulin, O. Shuosi and J. Zhao, Potential application of pristine and Al-doped graphyne-like BN nanosheet for detection of anticancer fluorouracil drug, *J. Mol. Model.*, 2020, **26**(7), 169.
14 H. O. Edet, *et al.*, Heteroatoms (B, N, S) doped quantum dots as potential drug delivery system for isoniazid: insight from DFT, NCI, and QTAIM, *Heliyon*, 2023, **9**(1), e12599–e12614, DOI: 10.1016/j.heliyon.2022.e12599.
15 M. A. Ibrahim, *et al.*, A comparative DFT investigation of the adsorption of temozolomide anticancer drug over beryllium oxide and boron nitride nanocarriers, *ACS Omega*, 2024, **9**(23), 25203–25214.
16 Z. H. Al-Sawaff, S. S. Dalgic and F. Kandemirli, A DENSITY FUNCTIONAL THEORY (DFT) STUDY ON SILICON DOPED

CARBON NANOTUBE SI–CNT AS A CARRIER FOR BMSF-BENZ DRUG USED FOR OSTEOPOROSIS DISEASE, *Momento*, 2022, **65**, 1–24.

17 M. B. Kanoun and S. Goumri-Said, Insights into the impact of Mn-doped inorganic $CsPbBr_3$ perovskite on electronic structures and magnetism for photovoltaic application, *Mater. Today Energy*, 2021, **21**, 100796.

18 A. Shah, A. H. Munshi, A. P. Nicholson, A. Thiyagarajan, U. M. Pozzoni and W. S. Sampath, Atomistic modeling of energy band alignment in CdSeTe surfaces, *Appl. Surf. Sci.*, 2021, **544**, 148762.

19 A. M. Khudhair and A. Ben Ahmed, Adsorption Characteristics of the Anticancer Drug Hydroxyurea with Armchair BN Graphene Nanoribbons Containing and Lacking Vacancy Defects: Insight via DFT Calculations, *J. Supercond. Novel Magn.*, 2024, **37**(8), 1509–1518.

20 B. Chettri, P. K. Patra, Z. Renthlei, A. Laref and D. P. Rai, Bilayer heterostructure of boron nitride and graphene for hydrogen storage: a first-principles study, *Energy Fuels*, 2022, **36**(21), 13307–13316.

21 S. Grimme, J. Antony, S. Ehrlich and H. Krieg, A consistent and accurate ab initio parametrization of density functional dispersion correction (DFT-D) for the 94 elements H-Pu, *J. Chem. Phys.*, 2010, **132**(15), 154104, DOI: 10.1063/1.3382344.

22 A. M. Khudhair, A. B. Ahmed, F. N. Ajeel and M. H. Mohammed, Theoretical investigation on the therapeutic applications of C2B and C2O as targeted drug delivery systems for hydroxyurea and 6-thioguanine in cancer treatment, *Nano-Struct. Nano-Objects*, 2024, **38**, 101135.

23 J. Hostas and J. Rezac, Accurate DFT-D3 calculations in a small basis set, *J. Chem. Theory Comput.*, 2017, **13**(8), 3575–3585.

24 M. J. van Setten, *et al.*, The PseudoDojo: Training and grading a 85 element optimized norm-conserving pseudopotential table, *Comput. Phys. Commun.*, 2018, **226**, 39–54.

25 J. P. Perdew, K. Burke and M. Ernzerhof, Generalized gradient approximation made simple, *Phys. Rev. Lett.*, 1996, **77**(18), 3865.

26 F. N. Ajeel, K. H. Bardan, S. H. Kareem and A. M. Khudhair, Pd doped carbon nanotubes as a drug carrier for Gemcitabine anticancer drug: DFT studies, *Chem. Phys. Impact*, 2023, **7**, 100298.

27 F. N. Ajeel, M. N. Mutier, K. H. Mohsin, S. K. Khamees, A. M. Khudhair and A. B. Ahmed, Theoretical Study on Electronic Properties of BN Dimers Doped Graphene Quantum dots, *Bionanoscience*, 2024, 1–9.

28 A. M. Khudhair, F. N. Ajeel and M. H. Mohammed, Theoretical study of the electronic and optical properties to design dye-sensitivity for using in solar cell device, *Russ. J. Phys. Chem. B*, 2018, **12**, 645–650.

29 F. N. Ajeel, M. H. Mohammed and A. M. Khudhair, SWCNT as a model nanosensor for associated petroleum gas molecules: via DFT/B3LYP investigations, *Russ. J. Phys. Chem. B*, 2019, **13**, 196–204.

30 F. N. Ajeel, Y. W. Ouda and A. M. Khudhair, Graphene Nanoflakes as a New Nanobiosensor for Histidine Amino Acid in Fish with Gas, Ethanol, DMSO and Water Environment, *J. Basrah Res.*, 2019, **45**(2A), 1–6.

31 A. M. Khudhair and A. Ben Ahmed, Pure and stone-wales defect armchair boron nitride graphene nanoribbons as anticancer drug delivery vehicles: a theoretical investigation, *J. Cluster Sci.*, 2024, **35**(2), 451–460.

32 F. Mollania, N. L. Hadipour and N. Mollania, CNT-based nanocarrier loaded with pyrimethamine for adipose mesenchymal stem cells differentiation and cancer treatment: The computational and experimental methods, *J. Biotechnol.*, 2020, **308**, 40–55.

33 S. Keshtkar, *et al.*, A novel highly sensitive and selective H_2S gas sensor at low temperatures based on SnO_2 quantum dots-C_{60} nanohybrid: experimental and theory study, *Talanta*, 2018, **188**, 531–539.

34 C. Xiao, K. Ma, G. Cai, X. Zhang and E. Vessally, Borophene as an electronic sensor for metronidazole drug: a computational study, *J. Mol. Graphics Modell.*, 2020, **96**, 107539.

35 N. L. Hadipour, A. Ahmadi Peyghan and H. Soleymanabadi, Theoretical study on the Al-doped ZnO nanoclusters for CO chemical sensors, *J. Phys. Chem. C*, 2015, **119**(11), 6398–6404.

36 K. H. Bardan, F. N. Ajeel, M. H. Mohammed, A. M. Khudhair and A. B. Ahmed, DFT study of adsorption properties of the ammonia on both pristine and Si-doped graphene nanoflakes, *Chem. Phys. Impact*, 2024, **8**, 100561.

37 M. Liedke, K. Potzger, N. Srinivasan and A. Wagner, Publications Repository-Helmholtz-Zentrum Dresden-Rossendorf.

38 A. M. Khudhair and A. B. Ahmed, First investigation survey on the pristine C_3N_3 and B_3O_3 monolayer as a promising vehicle for delivery of 5-fluorouracil and cisplatin anticancer drugs, *Chin. J. Phys.*, 2025, **95**, 674–684.

39 A. M. Khudhair, I. Dhouib, F. N. Ajeel, A. B. Ahmed and B. Khemakhem, A Novel Al8N8 and B8N8 Nanoring Monolayer for Sensing and Drug Delivery of Cisplatin and Nitrosourea Anticancer Drugs: A DFT Insight, *J. Inorg. Organomet. Polym. Mater.*, 2025, 1–14.

40 L. L. Bechohra, M. Kurban, N. E. H. Medigue and S. Kellou-Taïri, Drug delivery potential of carbon and boron nitride nanotubes: A DFT-D3 analysis of curcumin binding interactions, *Diamond Relat. Mater.*, 2024, **149**, 111626–111643, DOI: 10.1016/j.diamond.2024.111626.

41 A. Maurya, *et al.*, Drug delivery potential of γ-graphyne, 6,6,12-graphyne and γ-graphdiyne for 5-Fluorouracil: insights from DFT calculations, *Compos. Interfaces*, 2025, **32**(8), 1193–1213, DOI: 10.1080/09276440.2025.2460350.

42 A. Maurya, *et al.*, A Novel Pyridopyrimidine Derivative as a Potential Breast Cancer Agent: DFT, Docking, MD Simulation, and Cytotoxic Studies, *Chem. Biodiversity*, 2025, **22**(12), e01955, DOI: 10.1002/cbdv.202501955.

43 K.-i Murata and H. Tanaka, Liquid–liquid transition without macroscopic phase separation in a water–glycerol mixture, *Nat. Mater.*, 2012, **11**(5), 436–443.

44 T. Sahoo and P. Kale, Work function-based metal–oxide–semiconductor hydrogen sensor and its functionality: a review, *Adv. Mater. Interfaces*, 2021, **8**(23), 2100649.

45 J.-X. Zhang and G.-H. Yang, Low-computation adaptive fuzzy tracking control of unknown nonlinear systems with unmatched disturbances, *IEEE Trans. Fuzzy Syst.*, 2019, **28**(2), 321–332.
46 S. Ajmal, *et al.*, Electron deficient boron-doped amorphous carbon nitride to uphill N_2 photo-fixation through π back donation, *Appl. Catal., B*, 2023, **321**, 122070.
47 E. Caillosse, *et al.*, Photo-induced self-assembly of silver nanoparticles for rapid generation of first and second surface mirrors, *ACS Appl. Nano Mater.*, 2020, **3**(7), 6531–6540.
48 L. Chen, J. T. Ren and Z. Y. Yuan, Enabling internal electric fields to enhance energy and environmental catalysis, *Adv. Energy Mater.*, 2023, **13**(11), 2203720.
49 G. Speranza, Carbon nanomaterials: Synthesis, functionalization and sensing applications, *Nanomaterials*, 2021, **11**(4), 967.
50 P. Verma, A. Srivastava, P. Prajapati, P. Tandon and M. R. Shimpi, Molecular structure, hydrogen bonding interactions and docking simulations of nicotinamide (monomeric and trimeric models) by using spectroscopy and theoretical approach, *Polycyclic Aromat. Compd.*, 2024, **44**(3), 1537–1555.
51 O. C. Godfrey, *et al.*, Impact of polar (DMSO, ethanol, water) solvation on geometry, spectroscopy (FT-IR, UV, NMR), quantum chemical parameters, and the antifungal activities of benzothiazole derivative by molecular docking approach, *Chem. Phys. Impact*, 2023, **7**, 100349.
52 R. Meenakshi, Spectral investigations, DFT based global reactivity descriptors, Inhibition efficiency and analysis of 5-chloro-2-nitroanisole as π-spacer with donor-acceptor variations effect for DSSCs performance, *J. Mol. Struct.*, 2017, **1127**, 694–707.
53 A. I. Väkeväinen, A. J. Moilanen, M. Nečada, T. K. Hakala, K. S. Daskalakis and P. Törmä, Sub-picosecond thermalization dynamics in condensation of strongly coupled lattice plasmons, *Nat. Commun.*, 2020, **11**(1), 3139.
54 G. J. Martyna, M. L. Klein and M. Tuckerman, Nosé–Hoover chains: The canonical ensemble via continuous dynamics, The, *J. Chem. Phys.*, 1992, **97**(4), 2635–2643.
55 D. M. Long, J. A. Greathouse, G. Xu and K. L. Jungjohann, Molecular dynamics simulation and cryo-electron microscopy investigation of AOT surfactant structure at the hydrated mica surface, *Minerals*, 2022, **12**(4), 479.
56 S. K. Jana, N. N. Som and P. K. Jha, Size-dependent fullerenes for enhanced interaction of l-leucine: a combined DFT and MD simulations approach, *Langmuir*, 2024, **40**(27), 13844–13859.
57 Z. Shariatinia and M. Kurban, Sustainable Design of Green-Functionalized π-Conjugated BTBF-DPA Derivatives for High-Mobility Hole Transport, *Tetrahedron*, 2025, 134984.
58 H. Kurban, P. Sharma, M. M. Dalkilic and M. Kurban, Accelerating density of states prediction in Zn-doped MgO nanoparticles via kernel-optimized weighted k-NN, *Sci. Rep.*, 2025, **15**(1), 30524.
59 R. Sainda, S. K. Jana and P. K. Jha, Multiscale simulation of pesticides adsorption on passivated carbon nanotubes, *Diamond Relat. Mater.*, 2025, 113279.
60 A. Bunker and T. Róg, Mechanistic understanding from molecular dynamics simulation in pharmaceutical research 1: drug delivery, *Front. Mol. Biosci.*, 2020, **7**, 604770.
61 X. Xu, *et al.*, Application of molecular dynamics simulation in self-assembled cancer nanomedicine, *Biomater. Res.*, 2023, **27**(1), 39.